Mapping the Structural Requirements for Nicotinic Acetylcholine Receptor Activation by Using Tethered Alkyltrimethylammonium Agonists and Antagonists†

Deirdre S. Stewart, David C. Chiara, and Jonathan B. Cohen*

Department of Neurobiology, Harvard Medical School, Boston, Massachusetts 02115

Received April 7, 2006; Revised Manuscript Received July 13, 2006

ABSTRACT: A molecule as simple in structure as tetramethylammonium gates the nicotinic acetylcholine receptor (nAChR) with high efficacy. To compare the structure of the nAChR transmitter binding site in the open channel state with that of the ACh binding protein, we determined the efficacy of nAChR gating by $-S(CH_2)_nN(CH_3)_3^+$ ($n = 1-4$) tethered to substituted cysteines at positions in the α subunits or γ and δ subunits predicted to contribute to the ACh binding sites in mutant *Torpedo* nAChRs expressed in *Xenopus* oocytes. For tethered thiocholine [$-S(CH_2)_2N(CH_3)_3^+$], we previously reported that within α195−201 gating was observed only at αY198C while at αY93C it acted as an antagonist. We now show that within α191−194, thiocholine activates when tethered at αCys192 or αCys193. Thiocholine also activates when tethered at αY190C or αW149C in nAChRs containing a β subunit mutation (βL257S) that destabilizes the closed channel, but not from γW55C/δW57C, where longer adducts can activate. When tethered at positions in binding site segment E, thiocholine activates only from γL119C/δL121C, where the shorter $-S(CH_2)_1N(CH3)_3^+$ acts as an antagonist. Longer adducts tethered at γL109C/δL111C or γL119C/δL121C also activate, but less efficiently. The length requirements for efficient gating by tethered agonists agree closely with predictions based upon the structure of the agonist site in a nAChR homology model derived from the ACh binding protein structure, which suggests that this structure is an excellent model of the nAChR agonist binding site in the open channel conformation. The inability of thiocholine to activate from αY93C, which is not predicted by the model, is discussed in terms of the structure of the nAChR in the closed state.

The "cystine-loop" superfamily of transmitter-gated ion channels includes nicotinic acetylcholine receptors (nAChRs)[1] and serotonin 5-HT_3 receptors, containing cation selective channels, as well as $GABA_A$ and glycine receptors with anion selective channels (*1*−*4*). These receptors are each made up of five identical or homologous transmembrane subunits associated about a central axis that forms the ion channel, and their transmitter binding sites are located in the extracellular domain at subunit interfaces. The nAChRs of vertebrate skeletal muscle and the electric organs of a marine ray, *Torpedo*, have a subunit stoichiometry of $\alpha_2\beta\gamma\delta$, and the transmitter binding sites are at the α−γ and α−δ subunit interfaces.

The structure of the extracellular (N-terminal) domain of a nAChR is homologous to that of the snail acetylcholine binding protein (AChBP), a soluble homopentamer with a subunit core organized as a hydrophobic β-sandwich and the transmitter binding sites at a position that in the nAChR would be 30 Å above the bilayer (*5*, *6*). The AChBP structure has been used to refine to 4 Å resolution the structure of the *Torpedo* nAChR transmembrane and extracellular domains in the absence of agonist (*7*, *8*). The transmitter binding sites in the AChBP and nAChR are formed by amino acids from three noncontiguous stretches of primary structure of one subunit (segments A−C, nAChR α subunit) and from two regions of the adjacent subunit (segments D and E, nAChR γ or δ subunit). In the AChBP, five aromatic amino acids from segments A−D form a core aromatic "pocket" with a dimension optimal for accommodation of a trimethylammonium group. The binding site is "capped" by a vicinal disulfide (nAChR αCys192/193) forming the turn between antiparallel β strands 9 and 10 (segment C), and the amino acids in the γ or δ subunit closest to the aromatic pocket are on three antiparallel β strands that form part of a rigid four-strand β sheet. In contrast, for the nAChR in the absence of agonist, there is a reorientation of binding site segments A−C resulting in the absence of the highly structured, core aromatic pocket (*7*, *8*).

The ACh binding site structure of the AChBP in the presence of HEPES or agonist (*5*, *6*) is likely to approximate the structure of the nAChR transmitter binding sites in receptor conformations with high affinity for agonist, i.e., the open channel state and/or a desensitized state. One

† This research was supported in part by United States Public Health Service Grants NS 19522 and GM-58448.

* To whom correspondence should be addressed: Department of Neurobiology, Harvard Medical School, 220 Longwood Ave., Boston, MA 02115. Telephone: (617) 432-1728. Fax: (617) 734-7557. E-mail: jonathan_cohen@hms.harvard.edu.

[1] Abbreviations: ACh, acetylcholine; AChBP, acetylcholine binding protein of *Lymnea stagnalis*; nAChR, nicotinic acetylcholine receptor; α-BgTx, α-bungarotoxin; TMA, tetramethylammonium; MTS, methanethiosulfonate; $MTSC_nTMA$, [*n*-(trimethylammonium)$(CH_2)_n$]methanethiosulfonate, where $n = 1-4$; $MTSC_2TEA$, [2-(triethylammonium)-ethyl]methanethiosulfonate; MTSEA, 2-aminoethylmethanethiosulfonate; MTSPrCh, 2-carboxyethylmethanethiosulfonate, choline ester; MBTA, 4-(*N*-maleimido)benzyltrimethylammonium; BrACh, bromoacetylcholine; TCEP, tris(2-carboxyethyl)phosphine.

10.1021/bi060686t CCC: $33.50
Published on Web 08/15/2006

method of testing this experimentally is to determine whether the structural requirements for tethered agonists in a nAChR are consistent with predictions based upon the distance relations within the AChBP structure. A molecule as simple as tetramethylammonium (TMA) gates the nAChR with high efficacy, albeit with low potency (*9*, *10*). Bromoacetylcholine acts as a tethered agonist after reaction with αCys192 or αCys193 in reduced, native nAChRs (*11*, *12*), and thiocholine acts as an agonist when tethered at αY198C but not at other positions of Cys substitution within α195−201 or at αY93C (*13*, *14*).

In this report, we express Cys mutant *Torpedo* nAChRs in *Xenopus* oocytes and tether alkyltrimethylammonium compounds of varying chain length in the γ and δ subunits near the ACh binding sites or at additional positions in the α subunits (α188−194 and α149) to determine distance relations that are important for activation. Functional properties are compared for mutant nAChRs after reaction with trimethylammonium-alkyl-methanethiosulfonates (MTSs) of varying chain length (MTSC$_n$TMAs), bromoacetylcholine, and MTSpropionylcholine (MTSPrCh). Since each CH_2 group increases the maximal length of the tether by 0.8 Å, comparison of responses for tethered $-S(CH_2)_nN(CH_3)_3^+$ (n = 1−4) allows a definition at angstrom resolution of the orientation of the positive charge relative to the binding site amino acids. Comparison of the length requirements for gating reported here and in previous studies (*13*, *14*) with the tether lengths necessary to position the positive charge in the center of the aromatic box forming the transmitter binding site in the nAChR homology model based on the AChBP indicates that this structure provides an excellent model of the structure of the nAChR ACh site associated with channel gating. However, the structure does not predict the observed inability to activate when tethered at αY93C, which is better understood by consideration of the structure of the nAChR transmitter binding site in the absence of agonist.

EXPERIMENTAL PROCEDURES

cDNA Mutagenesis. Construction of the nAChR αY93C, αW149C, αY190C, αY198C, γW55C, γE57C, γN107C, γL109C, and γY113C mutants was described previously (*13*, *14*). Most new subunit mutants were constructed by "overlap extension" PCR using *Torpedo californica* nAChR subunit plamids (α, γ, and δ in pMXT and β in pSP64) as described previously (*13*). The α subunit mutants αV188C, αY189C, αT191C, αC193S, and αP194C were generated using primers which gave a PCR product of ∼1200 bp that was subcloned using the unique restriction sites BsiWI and BbsI of the α subunit coding region. Single Cys substitutions within γ114−121 were generated in an ∼1100 bp PCR product that was subcloned using the HindIII site in the vector and the unique StuI site in the γ coding region. The δ subunit mutants (N109C, L111C, and L121C) were generated using primers which gave an ∼500 bp PCR product that was subcloned using the unique BspEI and BstBI restriction sites within the δ subunit coding region. PCRs were for 24 cycles with a three-step protocol: 1.5 min at 94 °C, 2 min at 42 °C, and 2 min at 72 °C. The βL257S (βM2−9) mutant was generated using primers which gave an ∼600 bp PCR product after a reaction for 1.5 min at 95, 45, and 72 for 24 cycles. That PCR fragment was subcloned using the unique BsiWI and BstXI restriction sites within the β subunit coding region. GIBCO PCR Super Mix High Fidelity was used in the reactions as specified by the manufacturer's protocol. PCR products were purified and DNA enzymatic reactions performed as described previously (*13*). αC192S, αC192S/αC193S, δW57C, δD59C, δT119C, and δP123C mutants were constructed using the Quick Change site-directed mutagenesis kit (Stratagene). Oligonucleotide primers were purchased from Invitrogen LifeTechnologies. Bio-Rad miniprep kits were used to propagate plasmid DNA. Mutants constructed using overlap extension were confirmed by sequencing (Biopolymers Facility, Howard Hughes Medical Institute, Harvard Medical School) through the PCR region, and mutants prepared by the Quick Change method were confirmed by sequencing the entire coding region.

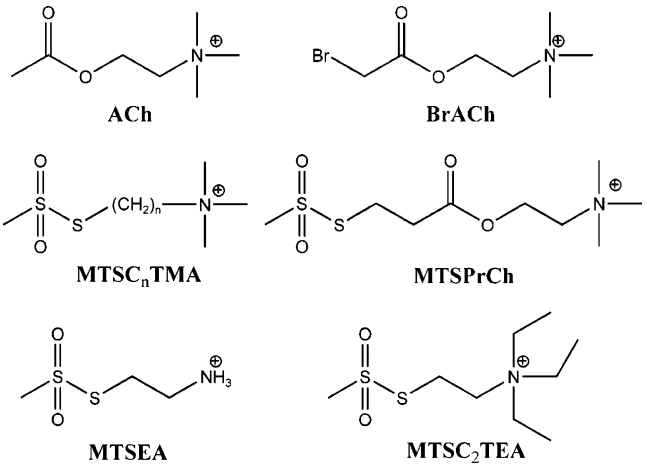

FIGURE 1: Structures.

Electrophysiology. In vitro transcription of *T. californica* nAChR subunit specific cRNAs as well as the protocols for the isolation and injection of *Xenopus laevis* oocytes and the measurement of nAChR responses by two-electrode voltage clamp were carried out as described previously (*13*). The Cys mutant nAChR subunit RNA was mixed with the appropriate wild-type subunit RNAs at a 2α/β/γ/δ molar ratio. Isolated, follicle-free oocytes were injected with 0.5−10 ng of subunit specific RNAs, and the currents elicited by ACh were measured 24−72 h later. Salts, atropine, ACh, and bromoacetylcholine were from Sigma (St. Louis, MO). MTS reagents (Figure 1, MTSC$_1$TMA, MTSC$_2$TMA, MTSC$_3$-TMA, MTSC$_4$TMA, MTSC$_2$TEA, MTSEA, and MTSPrCh) and maleimidobenzyltrimethylammonium (MBTA) were from Toronto Research Chemicals (North York, ON). Tris-(2-carboxyethyl)phosphine (TCEP) and Biotin-PEO maleimide were from Pierce (Rockford, IL). ACh dose−response curves were fit to the equation $I/I_{max} = [1 + (K_{app}/[ACh])^{n_H}]^{-1}$, where I and I_{max} are the currents at the specified concentration of ACh and the maximal current, respectively. K_{app} is the apparent activation constant for ACh, and n_H is the Hill coefficient. PCLAMP (Axon Instruments, Foster City, CA) and SigmaPlot (SPSS Inc., Chicago, IL) were used for data analysis.

Rate Constants of nAChR Modification. Rate constants for covalent modification of Cys mutant nAChRs were determined, as previously described (*13*), in three ways depending on the nature of the response after modification: by the reduction of the ACh response after modification, by the dose-dependent increase in the sustained current response

after washout of the modifier, or upon modification by BrACh or MTSPrCh, by the decrease in reversible current response. Data were fit to the equation $I_t = I_\infty + (I_o - I_\infty) \exp(-t/\tau)$, where I_t is the current after modification for t seconds, I_∞ is the current remaining after the reaction is complete, and I_o is the initial current level. $1/\tau$ is the pseudo-first-order rate constant, and the second-order rate constant, k (mM^{-1} s^{-1}), is $(1/\tau)/x$, where x is the concentration of the modifying reagent. We refer to "maximal modification" of a receptor when further application of the modifying agent produces no further change in the measured response. For modifications resulting in nAChR activation or partial inhibition of ACh responses, we do not know the fraction of nAChRs actually modified, which could be determined only by experimental procedures beyond the scope of this study.

Surface nAChR Labeling. To measure the level of surface expression of nAChRs, oocytes were incubated with 2.5 nM [^{125}I]-α-BgTx (2000 Ci/mmol; Amersham Pharmacia Biotech) for 2 h at room temperature as described previously (*13*), and binding to individual oocytes was assessed by γ counting. Gating efficiencies of the expressed nAChRs (microamperes per femtomole of α-BgTx) were determined by quantifying in parallel for approximately five oocytes the maximal current responses to ACh and surface [^{125}I]-α-BgTx binding. For these assays, oocytes were injected with 10 ng of subunit RNAs, which for wild-type nAChRs and most mutants resulted in maximal ACh responses exceeding the capacity of the voltage clamp. In those cases, ACh was used at concentration (1−10 μM) giving a response within a reliable voltage clamp range, and the maximal response was calculated using those measurements and the K_{app} and Hill coefficient characteristic of that receptor. When [^{125}I]-α-BgTx binding was assessed in a single experiment for the oocytes injected with wild-type or mutant nAChR, the surface binding per oocyte usually varied by <20% (standard deviation), while expression levels varied substantially more in experiments carried out over the course of a year. For wild-type nAChRs, surface nAChR expression varied from 1 to 5 fmol of α-BgTx per oocyte when measured 2 days after injection, with maximal responses of usually between 20 and 60 μA/fmol of α-Bgtx.

nAChR Homology Model with Tethered Agonists and/or Antagonists. The crystal structure of the AChBP with bound carbamylcholine [PDB entry 1UV6 (*6*)] was used to create a homology model of the *T. californica* nAChR extracellular domain using Insight II (version 98; MSI, San Diego, CA) basically as described previously (*14*). The nAChR β and δ subunits and one of the α subunits were removed from the model, leaving the subunit pair forming the α−γ agonist binding site. The core aromatics in the homology model remained superimposed on those of the AChBP, while the positions of the sulfurs of αCys192 and -193 were shifted by ∼1.5 Å as a consequence of the additional amino acid in the nAChR sequence between αCys193 and αTyr198. To tether thiocholine within the transmitter binding site at a substituted Cys, it was first placed in the transmitter binding site with its $-N(CH_3)_3^+$ superimposed on that of carbamylcholine and its −SH oriented toward substituted Cys, and the disulfide bond was made. To relax the strained disulfide, the model was energy-minimized (Discovery module) by steepest descent until a local minimum was reached (rms derivative of 0.001) with freedom of movement only for the tethered ligand and the Cys side chain. To tether other ligands, the initial position of the thiocholine quaternary ammonium was maintained with the replacement molecule generated by removing a methylene or replacing the sulfur with the $-(CH_2)_nS$, followed by disulfide bond formation and minimization.

The Docking module was used to dock TMA in the same two-subunit α−γ agonist site model, with TMA initially placed in the aromatic box. The "binding site" was defined as any residue within 6 Å of the original placement of the positive charge of the bound carbamylcholine, and the protein was "charged" for the appropriate side chain ionization at pH 7.0. Structures were energy-minimized for 500 cycles, and 17 "unique" structures were collected which identified two distinct TMA binding sites, one inside the aromatic box (15 of 17) and the other outside the vicinal disulfide (2 of 17). Within the aromatic box, TMA was displaced by ∼0.6 Å from the charge of carbamylcholine in the AChBP in a direction toward αTyr93, αTrp149, and αTyr190. The positive charge was located 4.2 and 4.4 Å from the C^β atoms of αCys192 and -193, respectively; between 4.8 and 5.2 Å from the faces of the aromatic side chains of αTrp149, αTyr190, αTyr198, and γTrp55; 6.3 Å from that of αTyr93; and 5.5 Å from the closest atom on γLeu119. TMA outside the aromatic box was positioned 5.1 and 3.6 Å from the C^β atoms of αCys192 and -193, respectively, and 4.3 and 4.8 Å from the closest atoms on γLeu119 and γTyr117, respectively. When the docking was initiated with TMA in this outer site, this site was identified in 20 of 36 minimizations, while the site within the aromatic pocket was identified in 16 of 36 minimizations.

RESULTS

Functional Properties of Cys Mutant nAChRs. ACh dose responses were measured by two-electrode voltage clamp to determine K_{app} (the ACh concentration producing a half-maximal response), and the binding of [^{125}I]-α-BgTx to intact oocytes was assessed to quantify the level of nAChR surface expression (Table 1). For each mutant, the maximal current per surface nAChR (microamperes per femtomole of α-BgTx) was compared to the level determined in parallel for control oocytes expressing the wild-type nAChR.

Within ACh binding site segment C, single Cys substitutions were introduced at αVal188, αTyr189, αThr191, and αPro194, while αCys192 and αCys193 were mutated singly to Ser (αC192S and αC193S, respectively) to express nAChRs containing a single Cys at position α193 or α192. Although Mishina et al. (*15*) reported no detectable ACh responses for oocytes expressing αC192S or αC193S mutant nAChRs, we found that the αC192S and αC193S mutants, as well as the αC192S/αC193S double mutant, resulted in functional nAChRs with K_{app} values increased by 10−20-fold compared to that of the wild type. The αC192S and αC193S mutants, however, were characterized by low ACh responses unless the oocytes were first treated with the sulfhydryl reductant TCEP, a reducing agent that is not itself a thiol (*16*). Oocytes expressing these mutants were routinely treated with 10 mM TCEP for 10 s, which caused ∼2- and 10-fold increases in the maximal ACh response for the αC192S and αC193S mutants, respectively, without increas-

Table 1: Functional Properties of Mutant nAChRs[a]

nAChR	K_{app} (μM)	α-BgTx binding (% of WT)	I_{max}/nAChR (% of WT)
	Binding Site Segment C		
wild type	30 ± 8	100	100
αV188C	90 ± 10 (2)	60	50
αY189C	10 ± 2 (2)	30	50
αT191C	30 (1)	20	300
αC192S	470 ± 130	90	3[b]
αC193S	240 ± 60	50	8[b]
αP194C	15 ± 2	4	100
αC192S/αC193S	550 ± 40 (1)	350	2
	Binding Site Segment E		
γN107C/δN109C	34 ± 7 (1)	10	350
γN107C	35 ± 14	70	200
δN109C	21 ± 1 (1)	25	80
γL109C/δL111C	90 ± 40	50	70
γL109C	100 ± 20	70	200
δL111C	ND[c]	60	200
γY117C/δT119C	100 ± 10 (2)	10	170
γY117C	ND[c]	90	30
δT119C	60 (1)	10	160
γL119C/δL121C	50 ± 10	50	30
γL119C	40 ± 20	120	120
δL121C	56 ± 3	70	120
γP121C/δP123C	280 (1)	25	50

[a] ACh dose−response curves were measured and fit as described in Experimental Procedures, with the tabulated K_{app} values representing the mean ± standard deviation determined from at least three oocytes unless indicated. The efficiency of expression of each mutant nAChR on the oocyte surface was determined by assessing the binding of [^{125}I]-α-BgTx to intact oocytes in parallel with that for wild-type nAChRs. For each mutant, the response per surface nAChR was determined by measuring in parallel the maximal ACh responses and [^{125}I]-α-BgTx binding as described in Experimental Procedures. Values were normalized relative to the maximal ACh response per wild-type nAChR measured at the same time. Surface expression of wild-type nAChRs varied from 1 to 4 fmol of α-BgTx/oocyte, and maximal responses per nAChR varied from 20 to 60 μA/fmol of α-BgTx. [b] ACh responses measured after treatment of the oocyte with 10 mM TCEP. [c] Not determined.

ing the levels of surface α-BgTx binding, which were 50−100% of that of the wild type. After TCEP treatment, the maximal ACh responses per surface nAChR were only ~5% of that of the wild type and at a level similar to the responses of the αC192S/αC193S mutant. Treatment with TCEP did not increase the response for the other Cys mutants that were studied (except for αY190C; see later), and it had no effect on the ACh response for the αC192S/C193S mutant. For the αT191C and αP194C mutants, the K_{app} values were shifted less than 2-fold compared to that of the wild type, with the level of surface expression 5−20% of that of the wild type and a reduction in the maximal response to ACh. For the αV188C and αY189C nAChRs, the levels of surface expression and maximal ACh responses were ~50% of those of the wild type, with K_{app} values of 90 and 10 μM, respectively. Modification of αV188C by $MTSC_2TMA$ resulted in >95% inhibition of the subsequent ACh response, while the ACh response of the αY189C nAChR was unaffected. These two mutants were not characterized further.

Within ACh binding site segment E, we focused on four positions in the γ subunit and the corresponding positions in the δ subunit: γAsn107/δAsn109, γLeu109/δLeu111, γTyr117/δThr119, and γLeu119/δLeu119. Whether expressed as a γ subunit mutant with wild-type δ ($\gamma^m\delta^{wt}$), as $\gamma^{wt}\delta^m$, or as $\gamma^m\delta^m$, the ACh K_{app} values were increased by no more than 3-fold compared to that of the wild type. For the γN107C/δN109C and γY117C/δT119C mutants, the levels of surface expression were ~10% of that of the wild type, while the maximal ACh response per surface nAChR was similar to that of the wild type. For the γL109C/δL111C and γL119C/δL121C mutants, the levels of surface expression were 50−100% of that of the wild type, and the maximal responses per surface nAChR were ~50% of that of the wild type.

Within binding site segment D, we expressed as single or double mutants Cys-substituted γTrp55/δTrp57 or γGlu57/δAsp59. The K_{app} values for ACh of the γW55C (390 ± 70 μM)[2] and δW57C (250 ± 70 μM) mutants were increased by 10-fold compared to that of the wild type. For the γW55C/δW57C mutant, the ACh responses were too low for quantification of K_{app}, although the level of surface expression was as high as ~40% of that of the wild type. For the γE57C, δD59C, and γE57C/δD59C mutants, the ACh K_{app} values were shifted less than 1.5-fold from that of the wild type, and for the double mutant, the level of α-BgTx binding was ~60% of that of the wild type.

nAChR Activation from α191−194. Alkyltrimethylammonium derivatives of variable chain length were tethered by reacting αT191C, αC193S (αCys192), αC192S (αCys193), or αP194C mutant nAChRs with $MTSC_2TMA$, $MTSC_1$-TMA, or $MTSC_4TMA$. Maximal ACh responses were measured before and after exposure to the MTS reagent and a wash of 1−2 min. Representative current traces are shown in Figure 2, and data quantifying tethered ligand responses are presented later in Table 3. Modification of the αT191C and αP194C nAChRs by any of the three MTS reagents did not produce detectable activation. The ACh responses were inhibited by <30% after treatment, but the substituted Cys was accessible for modification, as evidenced by an ~50% reduction in the ACh response after modification by a biotin−PEO−maleimide species (not shown).

Tethering of thiocholine at αCys192 or αCys193, by reaction with $MTSC_2TMA$, resulted in inward currents that persisted for minutes and were ~75 and 30% as large as the reversible ACh response. With thiocholine tethered at αCys192 and in the presence of the sustained current, after maximal modification the ACh response was inhibited by >99%, while only partial inhibition of the ACh response (~30%) was seen when thiocholine was tethered at αCys193. Modification by $MTSC_1TMA$ also activated the nAChR from either position, with a higher efficacy from αCys192. At αCys192, tethering $-SC_1TMA$ inhibited the subsequent ACh response by >95%, while tethering at αCys193 inhibited the response by only 50%. Treatment with $MTSC_4TMA$ did not result in activation from either αCys192 or αCys193, and ACh responses were inhibited only for αCys192.

To further define the structural specificity for activation from αCys192 or αCys193, we examined responses after modification by MTSEA, which tethers $-S(CH_2)_2NH_3^+$, or $MTSC_2TEA$, which tethers $-S(CH_2)_2N(C_2H_5)_3^+$. Neither modification resulted in detectable activation (i.e., activation,

[2] This is in contrast to our previous characterization of the γW55C mutant (*13*), where the ACh K_{app} was within 2-fold of that of the wild type and no alteration of the ACh response was seen after treatment with $MTSC_2TMA$. Since the ACh K_{app} for a receptor lacking the γ subunit differs less than 2-fold from that of the wild type, we cannot determine retrospectively whether wild-type γ or a degraded mutant γ subunit RNA was used in error.

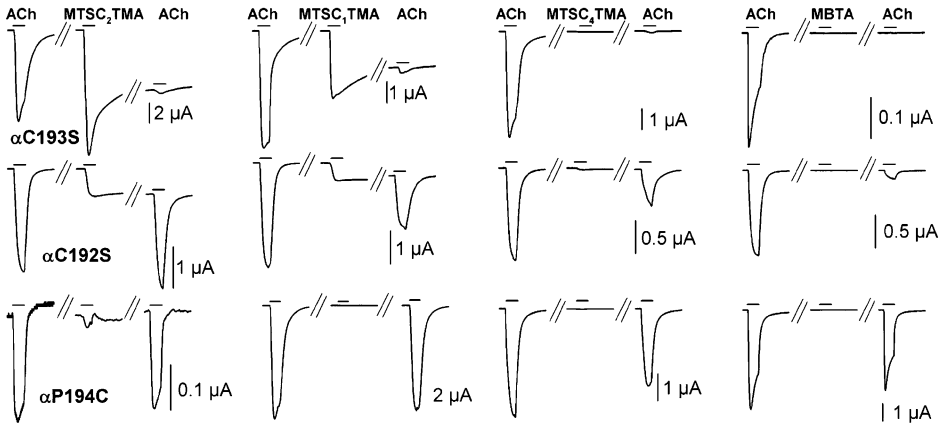

FIGURE 2: Responses of αC193S, αC192S, and αP194C mutant nAChRs after modification by MTSC$_n$TMA's and MBTA. ACh responses from oocytes expressing αC193S, αC192S (1 mM ACh, maximal response), or αP194C (10 μM ACh) nAChRs were measured before application of 100 μM MTS reagent or 1 mM MBTA for 5 s, and then after a wash of 30−60 s, ACh responses were retested. ACh test pulses were applied for 5 s and repeated at least four times. The horizontal bars indicate the 5 s duration of application of ACh or MTS reagent.

Table 2: Reaction Rate Constants of Mutant nAChRs with MTS Reagents, BrACh and MBTA[a]

	MTSC$_2$TMA	MTSC$_1$TMA	MTSC$_4$TMA	BrACh	MBTA
αCys192/αC193S	7800 ± 2700 (4)	9500 ± 5000 (2)	19000 ± 3000 (3)	0.2 ± 0.1 (4)	2500 ± 400 (3)
αC192S/αCys193	130 ± 60 (3)	ND[b]	400 (1)	<0.03 (3)	1700 (1)
γN107C/δN109C	0.9 ± 0.5 (2)	0.8 (1)	ND[b]	ND[b]	0.1 (1)
γL109C/δ111C	14 ± 4 (2)	8 (1)	24 (1)	ND[b]	40 (1)
γY117C/δT119C	0.2 (1)	1 (1)	2 (1)	ND[b]	0.2 (1)
γL119C/δL121C	1 ± 0.3 (6)	14 ± 4 (3)	0.5 ± 0.2 (3)	<0.05 (2)	0.5 ± 0.1 (2)

[a] Reaction rate constants, k (mM^{-1} s^{-1}) were determined as described in Experimental Procedures. The numbers in parenthesis are the number of oocytes used. [b] Not determined.

Table 3: Sustained Currents after Covalent Modification (%$I_{ACh,max}$)[a]

	-S(CH$_2$)$_n$N(CH$_3$)$_3$					
nAChR mutant [ACh K_{app} (μM)]	$n = 2$	$n = 1$	$n = 3$	$n = 4$	−S(CH$_2$)$_2$NH$_3^+$	−S(CH$_2$)$_2$N(C$_2$H$_5$)$_3$
γL119C/δL121C (53 ± 13)	**26 ± 10 (14)**	**0*** (4)	23 ± 6 (4)	**1.0 ± 0.6 (9)**	0***	**0.3 ± 0.2 (4)**
γN107C/δN109C [34 ± 7 (1)]	0** (3)	0** (2)	0** (1)	0*** (1)		
γL109C/δL111C (93 ± 40)	0** (6)	0** (2)	0** (1)	0.6 (2)		
γY117C/δT119C [104 ± 3 (2)]	0* (2)	0** (1)		0*** (3)		
γW55C/δW57C/β^m (1500 ± 200)	**0*** (4)		**3 ± 2 (3)**	50 ± 15 (5)	**0**** (1)	**0**** (1)
γE57C/δD59C (60 ± 20)	0*** (3)			0* (1)		
αY93C[b] (520 ± 30)	**0*** (4)	**0*** (4)	**0*** (3)		**0*** (11)	
αY93C/β^m (1100 ± 100)	**0***** (5)	**0**** (1)	**0*** (2)	**0.3 ± 0.1 (5)**	0*** (4)	0*** (1)
αW149C/β^m (3600 ± 1700)	60 ± 30 (5)	11 ± 1 (2)		80 ± 30 (3)	4 ± 2 (2)	13 ± 5 (3)
αY190C/β^m[c] (450 ± 190)	100 ± 25 (2)	250 (1)	120 (1)	70 (1)	0.7 ± 0.1 (2)	50 (1)
αC192/αC193S[c] (240 ± 60)	**70 ± 40 (5)**	**60 ± 10 (3)**	**25 ± 4 (2)**	**0.5 ± 0.3 (3)**	0**	0** (1)
αC192/αC193S/β^m[c] (90 ± 30)	**50 ± 20 (6)**			**3 (1)**		0**
αC193/αC192S[c] (470 ± 130)	22 ± 4 (4)	10 ± 4 (2)	7 ± 2 (2)	3 ± 2 (5)	0**	0** (1)
αC193/αC192S/β^m[c] (350 ± 120)	34 (1)					
αY198C (790 ± 10)	**470 ± 140[b] (19)**	**0** (<5%)[b] (8)	**75 ± 5[b] (6)**	**1.4 ± 0.1 (2)**	**0** (<2%)** (4)	
αY198C/β^m (680 ± 130)	**200 ± 90 (4)**	**15 (2)**	**80 (1)**	**1.9 ± 1.5 (5)**	**0**** (5)	**0**** (1)

[a] Sustained currents measured ~1 min after modification, expressed as a percent of the maximal, reversible ACh response before modification. Responses are means ± the standard deviation for data from the indicated number of oocytes. Values of K_{app} were determined from fits of the ACh dose response of the unmodified mutants for at least three oocytes. The sustained currents are indicated in bold when the ACh responses after modification were fully inhibited and the response had the properties expected for a tethered agonist. The other modifications resulted in either a >2-fold change in K_{app} or a partial inhibition of ACh responses. The zeroes indicate modifications that resulted in no detectable receptor activation, with the asterisks indicating the limit of detection, expressed as less than 1% of the maximal ACh response before modification (*, 1%; **, 0.2%; ***, 0.02%). Zeroes in bold font indicate a modification resulting in full inhibition of the subsequent ACh response. [b] Data from ref *13*. [c] Responses measured after treatment of the oocytes with 10 mM TCEP (see Results).

if it occurred, at a level that was <0.1% of that of ACh). For the αC193S mutant, modification by either reagent reduced ACh responses by >95%, while for αC192S, ACh responses were only partially inhibited (data not shown).

We compared the effects of the tethered −SC$_n$TMA's to those of MBTA, an antagonist, and BrACh, an agonist, the sulfhydryl reactive reagents first used to identify αCys192/αCys193 as a disulfide in the proximity of the agonist site (*17*, *18*). Reaction of MBTA with αCys192 or αCys193 inhibited ACh responses by >95% (Figure 2, right column). As for wild-type nAChR, BrACh acted as a potent reversible agonist for the mutants, producing maximal currents as large as that of ACh (Figure 3). BrACh tethered at either αCys192 or αCys193 also activated nAChRs, but much less efficiently

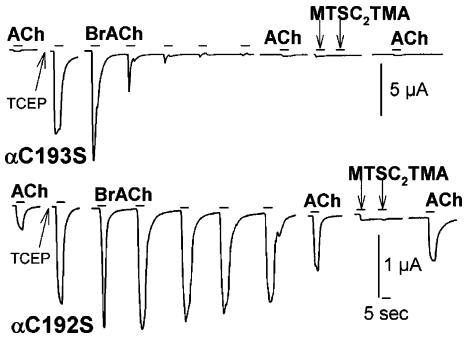

FIGURE 3: Responses of αC193S and αC192S mutant nAChRs after modification by BrACh. Oocytes expressing αC193S or αC192S nAChRs were tested with 1 mM ACh, then exposed to 10 mM TCEP for 10 s, and retested with 1 mM ACh. Repeated applications of 1 mM BrACh were followed by a 1 mM ACh test pulse, two applications of 100 μM MTSET, and a final 1 mM ACh test pulse. The horizontal scale bar is 5 s.

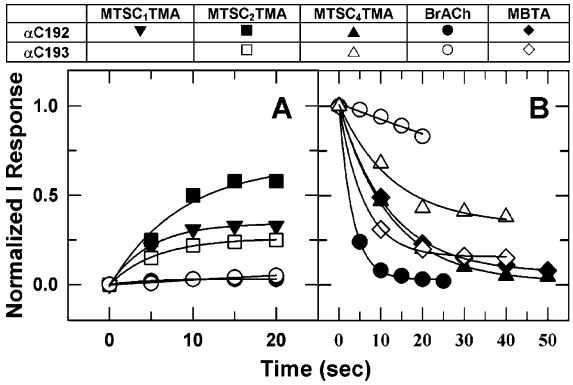

FIGURE 4: Kinetics of modification of αC193S and αC192S mutant nAChRs by $MTSC_nTMA$'s, MBTA, and BrACh. Symbols represent the current response plotted as a function of time of exposure to the MTS reagent. Plots were fit to a single-exponential function as described in Experimental Procedures to give the pseudo-first-order rate constant (τ) and the fractional response remaining after modification (I_∞). (A) Sustained current responses resulting from covalent activation. For αCys192 (αC193S), the cumulative sustained current responses to 10 nM $MTSC_2TMA$ (■) ($\tau = 8.3$ s, $I_\infty = 0.58$), 30 nM $MTSC_1TMA$ (▼) ($\tau = 5$ s, $I_\infty = 0.34$), and 1 mM BrACh (●) ($\tau = 4.3$ s, $I_\infty = 0.03$) are plotted as a function of time. For αCys193 (αC192S), the sustained current responses resulting from repeated applications of 1 μM $MTSC_2TMA$ (□) ($\tau = 5.6$ s, $I_\infty = 0.25$) and 1 mM BrACh (○) ($\tau = 333$ s, $I_\infty = 0.08$) are shown. Sustained current responses were normalized to the maximal ACh response for each oocyte. (B) Inhibition of ACh responses. For $MTSC_4TMA$ and MBTA, ACh responses were measured before and after application of reagent for 5 or 10 s and were normalized to the initial ACh response. For BrACh, the reversible current response was plotted as a function of time and normalized to the initial BrACh current. For αCys192 (αC193S), the effects of 1 mM BrACh (●) ($\tau = 3.3$ s, $I_\infty = 0.03$), 30 nM MBTA (◆) ($\tau = 12.1$ s, $I_\infty = 0.07$), and 5 nM $MTSC_4TMA$ (▲) ($\tau = 12.3$ s, $I_\infty = 0.02$) are shown. For αCys193 (αC192S), the effects of 1 mM BrACh (○) (not fit), 200 nM MBTA (◇) ($\tau = 5.9$ s, $I_\infty = 0.16$), and 200 nM $MTSC_4TMA$ (△) ($\tau = 12.8$ s, $I_\infty = 0.34$) are shown.

than tethered $-SC_2TMA$. Maximal modification of αCys192 resulted in persistent currents that were ~3% of that of ACh (or of the sustained response for tethered $-SC_2TMA$), while for αCys193, the sustained response was ~10% of that of ACh and 30% of that of tethered $-SC_2TMA$. Although the sustained currents are not readily apparent when plotted on the same scale as the reversible ACh or BrACh responses, the extent of covalent modification was readily followed during repeated applications in terms of the progressive reduction of the reversible response to BrACh as well as from the magnitude of the sustained response after subsequent modification by $MTSC_2TMA$ (Figure 3). As for the other modifiers that were tested, modification of αCys192 resulted in >95% inhibition of the subsequent ACh response, while modification of αCys193 resulted in only a partial reduction of the ACh response.

Kinetics of Modification of α*Cys192 and* α*Cys193.* The rates of covalent modification were determined by measuring the response to ACh after increasing reaction times or by measuring the increase in the sustained current as a function of reaction time (Figure 4), and the apparent bimolecular reaction rate constants were determined from the rates of reaction (Table 2). Reactions of the $MTSC_nTMA$'s at αCys192 were characterized by high reaction rate constants ($k \sim 10 \times 10^6$ M^{-1} s^{-1}), as seen for the modification of αCys192/Cys193 in reduced, wild-type nAChRs by $MTSC_2$-TMA or MBTA and 100-fold higher than for modification of free thiols in solution (*19*). The rate constants for modification of αCys193 were ~50-fold lower. Whether determined from the magnitude of the sustained response (Figure 4A) or from the kinetics of inhibition of the reversible response (Figure 4B), for BrACh the rate constant for modification of αCys192 ($k = 200$ M^{-1} s^{-1}) was at least 10-fold higher than that of αCys193, but each was 10000-fold lower than the rate constants for modification by the MTS reagents. For reaction of MBTA with either αCys192 or αCys193, k was equal to 2×10^6 M^{-1} s^{-1}, a value close to that for the MTS reagents reacting with αCys192.

nAChR Activation from γ*L119C/*δ*L121C.* On the basis of the nAChR homology model, for $-SC_2TMA$ tethered at γL119C/δL121C, the trimethylammonium can be oriented precisely within the center of the core aromatic binding pocket, and we predicted that it would act as a tethered agonist. In contrast, a similar fit would not be possible for $-SC_2TMA$ tethered at either γ107/δ109, γ109/δ111, or γ117/δ119, the positions adjacent to γ119/δ121 on antiparallel β strands 5′ and 6 that contribute to the entry to the binding pocket. Pairs of γ/δ Cys mutant subunits were coexpressed with wild-type α and β subunits, and the ACh responses of the mutant nAChRs were determined before and after exposure to $MTSC_nTMA$'s or MBTA (Figure 5). For each of these mutants, the K_{app} for ACh was increased no more than 3-fold compared to that of the wild type, and the efficiency of gating, as judged by the maximal ACh response per surface nAChR, varied by less than 3-fold from that of the wild type (Table 1).

For the γL119C/δL121C mutant (Figure 5, top), tethered $-SC_2TMA$ produced a sustained current that only slowly decreased on a time scale of minutes and was ~25% as large as the maximal, reversible response to ACh. After maximal modification, subsequent ACh responses were inhibited by >95%. In contrast, tethered $-SC_1TMA$ did not activate the γL119C/δL121C mutant, but subsequent ACh responses were inhibited by >95%. Reaction with $MTSC_4TMA$ resulted in inefficient gating, with sustained currents that were ~1% the ACh response (not shown), and tethered $-SC_4TMA$ reduced subsequent ACh responses by ≥95% (Figure 6). Reaction with MBTA resulted in no detectable sustained response, but even after maximal modification, ACh responses were only partially inhibited (Figure 6).

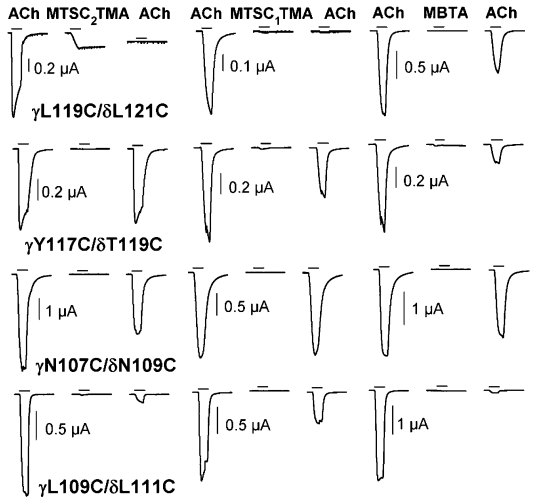

FIGURE 5: Responses of γL119C/δL121C, γY117C/δT119C, γN107C/δN109C, and γL109C/δL111C mutant nAChRs after modification by MTSC$_n$TMA's and MBTA. Oocytes expressing γ/δ Cys pairs were tested with ACh before and after a 10 s application of modifying reagent. MTS reagents were applied at a concentration of 100 μM for 10 s (two 5 s applications; one representative 5 s trace is shown). MBTA was applied at a concentration of 1 mM for 10 s (two 5 s applications). The concentration of the ACh test pulse depended on the expression level of the oocyte on the day of the experiment. For γL119C/δL121C, 300 μM ACh (maximal response) was used with MTSC$_2$-TMA, whereas 10 μM ACh was used with MTSC$_1$TMA and MBTA. For γY117C/δT119C, 1 mM ACh was used with MTSC$_2$-TMA, and 10 μM ACh was used with MTSC$_1$TMA and MBTA. For γN107C/δN109C, ACh concentrations of 10, 30, and 100 μM were used. For γL109C/δL111C, ACh concentrations of 10, 100, and 30 μM were used. Oocytes were washed for 30−60 s between each application. The horizontal scale bar is 5 s.

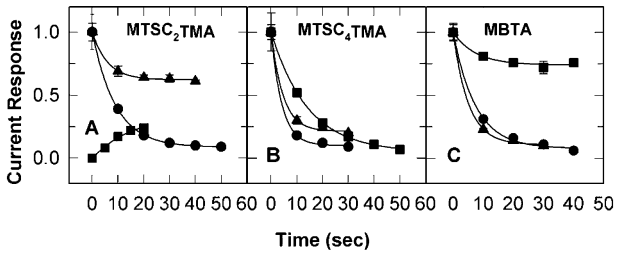

FIGURE 6: Kinetics of modification by MTSC$_n$TMA's and MBTA of γL109C/δL111C (●), γY117C/T119C (▲), and γL119C/δL121C (■) mutant nAChRs. Symbols represent either the ACh response remaining after modification for the indicated times or the sustained response due to covalent activation as explained in Figure 4 and Experimental Procedures. (A) MTSC$_2$TMA modification rates are shown for inhibition of the ACh responses for γ109/δ111 (10 μM, $\tau = 9$ s, $I_\infty = 0.09$) and γ117/119 (1 mM, $\tau = 6$ s, $I_\infty = 0.6$) and for the sustained response of γ119/L121 (100 μM, $\tau = 14$ s, $I_\infty = 0.25$). ACh responses were measured at 30 (●) or 100 μM (▲). (B) Inhibition by MTSC$_4$TMA of ACh responses at γ109/δ111 (10 μM, $\tau = 4$ s, $I_\infty = 0.1$), at γ119/121 (100 μM, $\tau = 18$ s, $I_\infty = 0$), and at γ117/δ119 (100 μM, $\tau = 4.5$ s, $I_\infty = 0.26$). ACh responses were measured at 30 (●) or 100 μM (▲ and ■). (C) Inhibition by MBTA of ACh responses at γ109/δ111 (3 μM, $\tau = 8$ s, $I_\infty = 0.08$), at γ119/δ121 (300 μM, $\tau = 7$ s, $I_\infty = 0.76$), and at γ117/δ119 (1 mM, $\tau = 5$ s, $I_\infty = 0.1$). ACh responses were measured at 30 (●) or 10 μM (▲ and ■).

We found no evidence of modification of γL119C/δL121C by BrACh (data not shown). Reaction with 0.1 mM BrACh for 20 s resulted in no sustained current and a <5% reduction in ACh responses. However, BrACh has low intrinsic reactivity, as evidenced by the reaction rate constants with

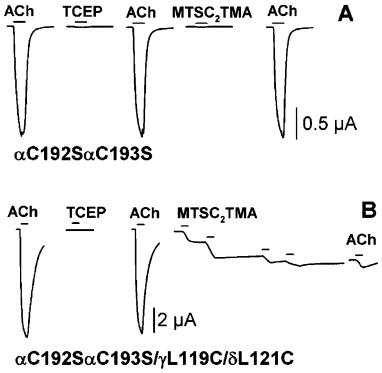

FIGURE 7: Responses of αC192S/αC193S and αC192S/αC193S/γL119C/δL121C mutant nAChRs after modification by MTSC$_2$-TMA. Oocytes expressing mutant nAChRs were first tested with 5 s 1 mM ACh applications, then treated for 10 s with 10 mM TCEP, and retested with 1 mM ACh. MTSC$_2$TMA (100 μM) was applied for 10 s (A, one 5 s application shown) or 20 s (B, four, 5 s applications), and the oocytes were then retested with 1 mM ACh. The horizontal scale bar represents 5 s.

αCys192 or αCys193 that were only 10^{-4} of that of the MTS reagents, and as we describe later, rate constants for reaction of MTS reagents with γL119C/δL121C were low ($k \sim 1 \times 10^3$ M^{-1} s^{-1}).

To rule out the possibility that the observed activation of the γL119C/δL121C mutant by tethered −SC$_2$TMA actually resulted from a modification of a free Cys at position α192 or α193 formed as a consequence of aberrant disulfide formation, we expressed the γL119C/δL121C mutant in the presence of α subunits lacking αCys192 or αCys193. The αC192S/αC193S mutant nAChR (containing wild-type non-α subunits) was expressed efficiently, with surface receptor levels 2−4-fold higher than that of the wild type. However, the ACh responses were similar to those of the αC192S or αC193S mutant, with the maximal response per surface nAChR being ∼2% of that of the wild type and K_{app} being ∼500 μM. For the αC192S/αC193S mutant, ACh responses were not significantly affected by TCEP or MTSC$_2$TMA (Figure 7A). Expression of the αC192S/αC193S/γL119C/δL121C mutant nAChR also resulted in functional receptors with surface receptor levels approximately double that of the wild type. The ACh K_{app} was similar to that for the αC192S/αC193S mutant, as were the maximal currents per surface receptor. As expected, treatment with TCEP did not alter the ACh responses. Reaction with MTSC$_2$TMA resulted in sustained currents the same in magnitude as the ACh response seen for the γL119C/δL121C mutant (Figure 7B).

Modification of Cys-Substituted γ117/119, γ107/δ109, and γ109/δ111. Each of these mutants was reacted with MTSC$_n$-TMA ($n = 1$, 2, and 4) and MBTA (Figures 5 and 6 and Table 3). Reaction with either MTSC$_1$TMA or MTSC$_2$TMA resulted in no detectable persistent currents. For MTSC$_4$-TMA, only reaction at γL109C/δL111C resulted in a small sustained current, ∼1% of that of ACh. Furthermore, reaction at these positions with the MTS reagents or MBTA generally resulted in a reduction, but not a complete inhibition, of the subsequent ACh responses. For γN107C/δN109C, all treatments resulted in a <30% reduction of the ACh responses. For γY117C/δT119C, after MTSC$_n$TMA treatment responses were inhibited by 40 −80%. For Cys-substituted γ109/δ111, the position on β strand 5 paired with γ117/δ119, maximal

modification by MBTA resulted in a >95% reduction of the ACh response. However, after maximal modification by $MTSC_2TMA$, ACh still bound and activated the nAChR, as shown by the fact that its K_{app} was increased by 10-fold to 800 μM and the maximal response reduced by only 70% (data not shown).

Reaction rate constants for the modification of the Cys mutant nAChRs were determined for three MTS reagents and MBTA (Table 2). Representative data are shown in Figure 6 for $MTSC_2TMA$, $MTSC_4TMA$, and MBTA. $MTSC_2TMA$ reacted at a low rate constant with γL119C/δL121C ($k = 1 \times 10^3$ M^{-1} s^{-1}), and 10-fold higher (γL109C/δL111C) or lower (γY117C/δT119C) at the other positions. The reaction rate constants for $MTSC_1TMA$, $MTSC_4TMA$, and MBTA were within a factor of 10 of those for $MTSC_2$-TMA.

Modification by MTSPrCh. While we wanted to use BrACh to tether acylcholine to the Cys mutant nAChRs, because of its low intrinsic reactivity, we were unable to find practical conditions for modifying the Cys mutant nAChRs other than αCys192 and αCys193 (Figure 3) or αY198C (*13*), i.e., cysteines that were characterized by very high reactivities with the MTS reagents ($k > 10^5$ M^{-1} s^{-1}). As an alternative, we tested MTSPrCh, which will tether thiopropionylcholine to Cys. It differs from the other MTS reagents in that it acted as a high-efficacy, reversible agonist of wild-type and αC192S/αC193S nAChRs, producing maximal responses that were ~50% of that of ACh with K_{app} values of ~80 μM. However, current responses were maximal at 300 μM and then decreased by 50% at 1 mM, most likely due to channel block. The inhibitory component at higher concentrations indicated that values of K_{app} and efficacy were probably underestimated.

Reaction of MTSPrCh with αCys192 or αCys193 resulted in sustained current responses that were ~20 and 80% of the ACh responses (Figure 8) and 3−5-fold larger than the sustained responses seen after modification by BrACh. The more efficient gating from αC193 contrasted with the results seen for $MTSC_1TMA$ and $MTSC_2TMA$, for which gating was more efficient after modification of αCys192. Reaction with MTSPrCh also resulted in persistent currents after modification of γL109C/δL111C or γY117C/δT119C that were ~5% of that of ACh, while for γL119C/δL121C, the responses were ~1% of that of ACh (or 3% as large as the persistent current after modification by $MTSC_2TMA$).

Modification of Cys-Substituted Binding Site Aromatics. We reported previously (*13*) that activation from αY198C by $-SC_2TMA$ produced sustained responses 5-fold higher than the maximal ACh response; tethered $-SC_4TMA$ gated only 1% as efficiently as ACh, and $-SC_1TMA$ acted only as an antagonist. For αY93C, reaction with $MTSC_nTMA$ ($n = 1-3$) inhibited only ACh responses. Modification of αW149C or αY190C was not studied because no ACh responses were detected. We have now reexamined functional properties of these mutants by coexpressing the binding site Cys mutant subunit with a mutant β subunit (β^m, βL257S at βM2−9) that destabilizes the closed channel in the absence of agonist (*20*, *21*). Spontaneous nAChR gating is seen for mutant nAChRs containing quaternary ammonium derivatives of tyrosine in place of αTrp149, αTyr93, or γTrp55/δTrp57 when coexpressed with β^m (but not wild-type β) (*22*, *23*). As for the mouse nAChR containing β^m and wild-type

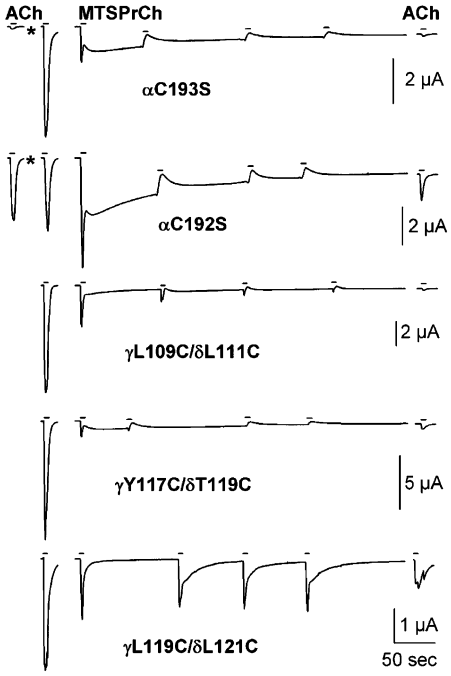

FIGURE 8: Responses of Cys mutant nAChRs after modification by MTSPrCh. Oocytes expressing αC192S and αC193S nAChRs were treated with 10 mM TCEP for 10 s (indicated with asterisks). ACh responses were measured at 1 mM, a concentration producing a maximal response for each mutant. For each mutant, MTSPrCh at 100 μM was applied for 20 s (in 5 s pulses), and then the ACh response was retested. The short horizontal scale bar represents 5 s.

α, γ, and δ subunits (*20*, *21*), we found for the *Torpedo* nAChR β^m mutant that the K_{app} for ACh was 3 μM, i.e., decreased 10-fold compared to that of the wild type, and the maximal currents per surface receptor were 2−4-fold higher than that of the wild type. For $\alpha_2\beta^m\gamma\delta$ or Cys mutant nAChRs containing the β^m subunit, there was no evidence of spontaneous channel gating in the absence of ACh or MTS reagent. At −70 mV, the holding currents were the same as those for wild-type nAChRs, and they were not reduced by the open channel blocker QX-222.

We first examined the effects of the β^m subunit on the responses to MTS modification of αY93C and αY198C nAChRs, for which ACh responses had been readily detected in the presence of the wild-type β subunit. The presence of β^m resulted in a <3-fold shift of ACh K_{app}, and the consequences of MTS modification were the same as those seen with the wild-type β subunit (Table 3). For αY93C/β^m, tethered $-SC_1TMA$ or $-SC_2TMA$ did not activate while subsequent ACh responses were inhibited by >95%. For αY198C/β^m, tethered $-SC_2TMA$ still activated with a 100-fold greater efficacy than $-SC_4TMA$ did.

ACh responses were readily detected in all oocytes expressing the αW149C/β^m and γW55C/δW57C/β^m mutants, with K_{app} values of 4 and 1.5 mM, respectively. For the αY190C/β^m mutant, ACh elicited maximal responses of ~1 μA with a K_{app} of 0.5 mM in ~40% of the oocytes that were tested (5 of 13), but maximal responses of only 10−30 nA were detected for the others. (No attempt was made to correlate the magnitude of the currents with the level of nAChR surface expression.) Treatment with TCEP doubled the maximal ACh responses for the αY190C/β^m mutant but did not alter the ACh response of the αW149C/β^m or

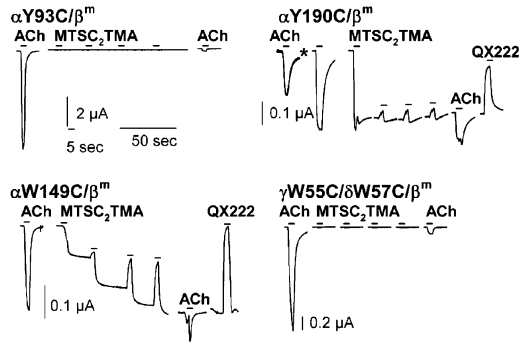

FIGURE 9: Responses of αY93C, αW149C, αY190C, and γW55C/δW57C mutant nAChRs after modification by $MTSC_2TMA$. In addition to a Cys substitution at one of the ACh binding site core aromatic side chains, each mutant nAChR also contained a mutation in the β subunit M2 ion channel domain (βLeu257Ser at βM2−9). ACh responses were measured at 0.1 (αY93C), 3 (αY190C and γW55C/δW57C), or 10 mM (αW149C). $MTSC_2TMA$ was applied for 20 s (in 5 s pulses) at 1 mM except for αY93C (0.1 mM), and then the ACh response was retested. For αY190C, 10 mM TCEP was applied for 20 s (indicated with an asterisk). The channel blocker QX-222 was applied for 5 s at 1 mM. The short horizontal scale bar represents 5 s.

γW55C/δW57C mutant. Representative current traces showing the effects of $MTSC_2TMA$ modification for these mutants and for αY93C/β^m are shown in Figure 9, with the results for the panel of MTS reagents included in Table 3. For the αW149C/β^m and αY190C/β^m mutants, sustained currents were seen after modification by each of the $MTSC_nTMA$'s, with the most efficient activation seen at αW149C for tethered $-SC_2TMA$ and $-SC_4TMA$ (currents that are ∼80% of that of ACh) and at αY190C for $-SC_1TMA$ and $-SC_2TMA$ (currents that are ∼100% of that of the ACh response). The open channel blocker QX-222 reversibly inhibited the sustained currents seen for $-SC_2TMA$. For both mutants, ACh responses after modification were reduced by 60−80%.[3] In contrast to the reactions of other ACh site Cys mutants that were studied, reaction at αW149C or αY190C with the primary amine MTSEA also activated, although the sustained currents were only ∼2% of that of ACh (Table 3). In addition, $-SC_2TEA$ tethered at either position activated, producing persistent currents similar in size to that seen for the $-SC_nTMA$'s.

The γW55C/δW57C/β^m mutant was not activated by treatment with $MTSC_1TMA$, $MTSC_2TMA$, MTSEA, or $MTSC_2TEA$, and subsequent ACh responses were inhibited by >95%. Reaction with $MTSC_4TMA$, however, did produce sustained currents ∼50% as large as the ACh response, with subsequent ACh responses inhibited by only ∼50% and with the K_{app} decreased from 1.5 to 0.2 mM (data not shown). We also tested responses of γE57C/δD59C and γE57C/δD59C/β^m mutant nAChRs to modification by $MTSC_2TMA$ or $MTSC_4TMA$. Neither modification activated the nAChR, and subsequent ACh responses were reduced. However, $-SC_2TMA$ tethered at γE57C/δD59C clearly acted as a modifier of nAChR gating rather than an inhibitor of ACh binding. After maximal modification by $MTSC_2TMA$, although the ACh maximal response was reduced by >93%, the K_{app} increased from 60 ± 30 to 530 ± 150 μM ($n = 3$).

nAChR Homology Model with Tethered Ligands. To relate our experimental results to the predicted orientations of tethered ligands in a *Torpedo* nAChR homology model based on the structure of the AChBP, single Cys substitutions were introduced into the homology model α or γ subunit (or αCys192 or αCys193 replaced with Ser), $-SC_nTMA$ was tethered to the Cys-SH as a strained disulfide, and the tethered ligand and Cys side chain were energy-minimized. Even though the length of the initial strained disulfides varied from 2.4 to >6 Å, after minimization the bond lengths were consistent with the S−S bond length of aliphatic disulfides (2 ± 0.06 Å), and the C−S−S−C dihedral angles were, unless noted, within 90 ± 15° (*24*−*27*). Shown in Figure 10B are $-SC_nTMA$'s ($n = 1$, 2, or 4) tethered at Cys-substituted γTrp55, γLeu109, or γLeu119, compared to the position of the positive charge of TMA docked in the homology model of the wild-type nAChR, with the charge displacements for those and other positions included in the figure legend. For $-SC_2TMA$ tethered at γL119C, from which it activated the nAChR, the positive charge was positioned 0.9 Å from that of TMA, while the displacement was 2.7, 3, and 4.5 Å when it was tethered at γW55C, γL109C, and γY117C, respectively, positions from which it did not activate. For $-SC_1TMA$ tethered at γL119C, where it functioned as an inhibitor, the charge was displaced by 1.8 Å, while for $-SC_4TMA$ tethered at γW55C (activation), γL109C (weak activation), and γY117C (no activation), the distances were 0.6, 1.1, and 1.6 Å, respectively. The displacements of the positive charge of $-SC_2TMA$ tethered to Cys substitutions within the α subunit were all ≤1 Å [αY93C (0.7 Å), αW149C (0.6 Å), αY190C (0.3 Å), αC192 (1.0 Å), αC193 (0.9 Å), and αY198C (0.2 Å)], with activation seen from each position other than αY93C.

DISCUSSION

In this study, we tested the capacity of alkyltrimethylammonium compounds to activate the nAChR when tethered at individually substituted cysteines at positions in the α subunits or γ and δ subunits that are predicted by the structure of the AChBP to be in or near the nAChR agonist binding site. With the maximal extended configuration of the tether changing by 0.8 Å with the addition (or removal) of a single CH_2, the results potentially define with angstrom resolution for each position the length requirement for activation. When positions from which tethers of varying chain length can activate are identified, the length of the shortest tether in its extended conformation provides a definition of a minimal distance for activation, while the longer, more flexible tether may not be in an extended conformation.

We found that depending upon the length of the tether, nAChRs can be either activated or inhibited by $-SC_nTMA$'s tethered at positions in the γ or δ subunit. As we describe below, the minimal length requirements for activation agree quite precisely with the tether lengths necessary to position

[3] After maximal modification of the αY190C/β^m mutant by $MTSC_2TMA$, subsequent ACh responses were reduced by ∼70% but were not fully inhibited. An ACh response after maximal modification by $MTSC_2TMA$ was also seen for the αC192S mutant (Figure 2). For both mutants before reaction with $MTSC_2TMA$, the responses to ACh doubled upon treatment with the reducing agent TCEP. Further studies are required to determine whether for these mutants the ACh response prior to TCEP treatment results in part from a subpopulation of surface nAChRs with a modified Cys not reactive with MTS reagents even after TCEP.

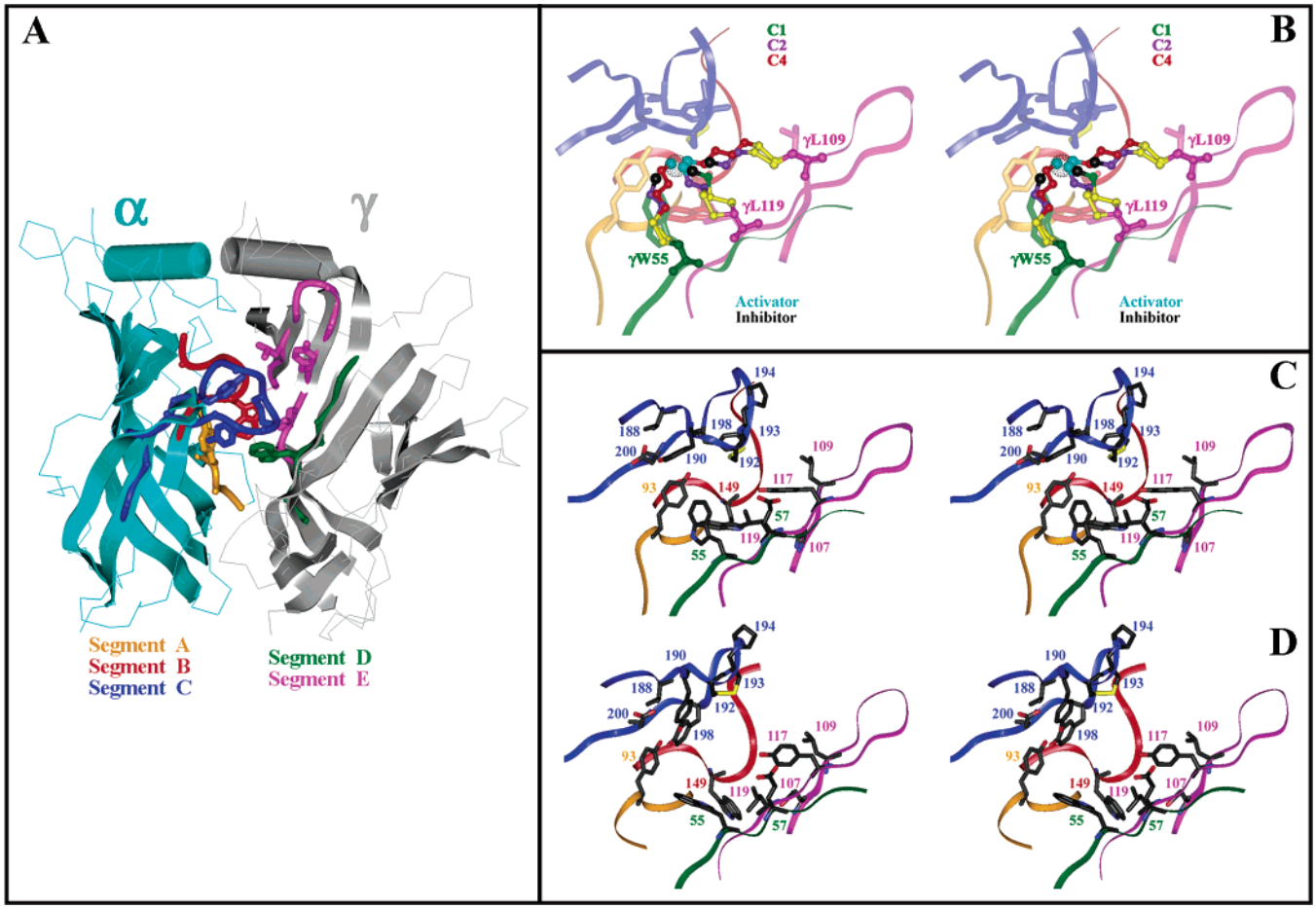

FIGURE 10: Stereo representation of the *Torpedo* nAChR agonist binding site at the α−γ interface with −SC$_n$TMA's tethered at substituted Cys residues. A homology model of the *Torpedo* nAChR extracellular domain was constructed from the AChBP structure with carbamylcholine bound (*6*). The regions of primary structure contributing to the transmitter binding site are drawn as color-coded ribbons for α subunit binding site segments A (gold), B (red), and C (blue) and γ subunit segments D (green) and E (magenta). (A) Shown are the primary sequence traces and secondary structural elements of two subunits, α (cyan) and γ (gray), with the ACh binding site at the subunit interface. (B) −SC$_n$TMA's were tethered to selected substituted Cys residues as described in Experimental Procedures. Drawn in stick format are the five binding site aromatic amino acids, the vicinal disulfide (sulfurs colored yellow), and the leucines at positions γ109 and γ119. Tethered −SC$_n$TMA's are shown in ball-and-stick format with the sulfur atoms colored yellow, the carbon linkers color coded to reflect their length (light green for $n = 1$, purple for $n = 2$, and red for $n = 4$), and the positively charged N drawn in the absence of the methyl groups and color-coded with regard to whether the tether activated (cyan) or inhibited (black) the receptor. The position of docking of TMA in the binding site of the wild-type nAChR is represented as a black sphere 2 Å in diameter. For −SC$_2$TMA tethered at γL119C, the positive charge is displaced by 0.9 Å from that of TMA, while from γW55C and γL109C, the displacements are 2.7 and 3.0 Å, respectively. For −SC$_1$TMA tethered at γL119C, the displacement is 1.1 Å. The charge displacements for −SC$_4$TMA tethered at γW55C and γL119C are 0.6 and 0.8 Å, respectively. The displacements (in angstroms) for −SC$_2$TMA at positions not shown are as follows: γE57C (2.4), γN107C (3.5), γL109C (3.0), γY117C (4.5), αY93C (0.7), αN94C (2.2), αW149C (1.0), αY190C (0.3), αC192 (1.0), αC193 (0.9), αP194C (6.3), αT196C (6.2), and αY198C (0.2). (C) nAChR homology model stereo representation of the α−γ transmitter binding site built from the AChBP. (D) Stereo representation of the α−γ transmitter binding site of the *Torpedo marmorata* nAChR in the absence of agonist (*8*), with the γ subunit amino acids numbered as for *T. californica*, which differs by a single amino acid insertion at the amino terminus of the mature subunit.

the positive charge in the center of the aromatic box forming the transmitter binding site in an nAChR homology model based upon the AChBP, which leads us to conclude that this structure is a good representation of the ACh binding site in an open channel state. Within the α subunit, both the activation from αW149C or from positions in binding site segment C (αY190C, αCys192, αCys193, or αY198C) and the inability to activate from the other positions between α188 and α200 are also generally consistent with the homology model, although the tether length requirements for activation are much less stringent than from positions in γ and δ subunits. The precise length requirements seen for activation from positions in binding site segments D and E of the γ and δ subunits most likely result from the rigidity of the γ/δ subunit β sheet scaffold contributing to the ACh binding site, in contrast to a greater flexibility associated with the orientation of the β strands forming α subunit binding site segment C. The inability of any tethered ligand to activate from αY93C cannot be simply explained from the homology model, but inspection of the structure of the nAChR in the closed state (*8*), which is undoubtedly the conformation that is being modified by the MTS reagents, provides a plausible explanation for this discrepancy.

Tethered Agonist and Antagonists versus Gating Modifiers. Our results demonstrate clearly that certain tethered ligands activate the nAChR, but it is important to consider the criteria that can be used to determine whether the activation occurs because the tethered quaternary ammonium acts as a tethered agonist occupying the ACh binding sites or alternatively acts as a modifier of gating without occupying and occluding the

transmitter binding site. In the latter case, after modification, ACh will still be able to bind and gate the nAChR, with the ACh dose response likely shifted as the modifier destabilizes the unliganded closed state relative to the open state or perturbs the microscopic rate constants of ACh association and/or dissociation or of channel opening or closing. Agonist-independent gating of wild-type nAChRs occurs with a very low probability, with the fraction in the open state in the absence of agonist less than 10^{-6} (*28*, *29*). However, single-channel analyses first identified substitutions within the ion channel domain that destabilize the closed state and greatly increase the level of agonist-independent gating (*20*, *21*). Those substitutions, when assayed by whole cell macroscopic currents, result in currents in the absence of agonist that can be inhibited by nAChR channel blockers and are characterized by decreases in the K_{app} for agonist-dependent gating. While many substitutions in or near the agonist binding site result in increased values of ACh K_{app} as a result of decreased channel opening rates or altered agonist binding (*4*), decreased K_{app} values were seen for Cys substitutions of nAChR αAsn95, αAla96, αPro197, and αLeu199 (*13*, *14*), which may reflect changes in agonist-independent gating as seen by single-channel analyses for many substitutions of mouse muscle nAChR αAsp97 (*30*).

When a tethered ligand activates the nAChR and prevents subsequent ACh responses, as was seen for $-SC_2TMA$ at γL119C/δL121C, the response is consistent with properties expected for a tethered agonist. In our studies, postmodification ACh responses were also fully inhibited for nAChRs activated by $-SC_2TMA$ tethered at αCys192 and αY198C, but not at αCys193, αW149C, or αY190C. Significantly, tethered $-SC_2TMA$ activated from αY198C, a mutation characterized by a K_{app} for ACh 20-fold greater than that of the wild type, but it did not activate from αP197C or αL199C, for which ACh K_{app} values were decreased by 5-fold (*14*); no activation was seen from αY93C even in nAChRs containing β^m (βL257S at βM2−9). Thus there is no correlation between activation by tethered $-SC_2TMA$ and the effect of the Cys substitution on the K_{app}.

Tethered $-SC_2TMA$ at αY93C or γW55C/δW57C did not activate nAChRs, and ACh responses were inhibited by >95%, as expected for a tethered antagonist. There were, however, positions where tethered $-SC_2TMA$ did not activate but acted clearly as a modifier of ACh gating. At γE57C/δD59C and γL109C/δL111C, when modification reduced maximal ACh responses by 93 and 70%, respectively, the ACh K_{app} values were increased by ∼10-fold.

For $-SC_1TMA$ tethered at γL119C/δL121C, which did not activate, subsequent ACh responses were reduced by >98%. While $-SC_1TMA$ tethered at γL119C/δL121C acted as expected for a tethered antagonist, $-SC_4TMA$ acted as a low-efficacy tethered agonist producing sustained currents that were ∼3% of the level seen for $-SC_2TMA$ and inhibiting ACh responses by ≥95%. Although $-SC_2TMA$ tethered at γW55C/δW57C acted as an antagonist inhibiting ACh responses by >95%, for $-SC_4TMA$, which activated, subsequent ACh responses were reduced by only 50% and the K_{app} was decreased from 1.5 to 0.2 mM. These results indicate that ACh is able to bind in the presence of $-SC_4TMA$ tethered at γW55C/δW57C, presumably because of the increased length and flexibility of the tether.

Headgroup Requirements for Gating. For wild-type muscle nAChRs, efficient gating is seen for TMA, while tetraethylammonium acts as a weak partial agonist with an efficacy that is <0.1% of that of ACh (*31*); there are no reports of activation by alkyl primary amines. In contrast to the activating responses seen for the tethered $-SC_nTMA$'s, activation was not seen for tethered $-SCH_2NH_3^+$, with the exception of the αW149C/β^m and αY190C/β^m nAChRs which were activated with an efficiency that was ∼1% of that of the optimal tethered $-SC_nTMA$. These mutants were also activated well by each of the $-SC_nTMA$'s and almost as well by $-SC_2TEA$, and ACh also gated the modified nAChRs. The limited structural specificity for activation of the αW149C/β^m and αY190C/β^m nAChRs and the activation by ACh in the presence of the tether suggests that for these mutants the tethered ligands are not acting as a tethered agonist but as a modifier of the equilibrium between closed and open states. The properties of these mutants appear to be similar to those containing quaternary ammonium analogues of tyrosine in place of αTyr93, αTrp149, or γTrp55/δTrp57 (*22*, *23*). For these mutant nAChRs, currents were seen in the absence of ACh. However, in each case, ACh further activated in the presence of the tethered positive charge, and spontaneous gating was also seen for the corresponding uncharged analogues containing a C in place of the N.

nAChR Activation and Desensitization. Our results establish that $-SC_2TMA$ tethered either at γL119C/δL121C or at certain positions in the α subunits acts as a tethered agonist, resulting in currents persisting for many minutes with little apparent desensitization. However, for those mutants, the responses to millimolar concentrations of ACh are also characterized by a reduced level of desensitization [<10% in 20 s (not shown)], so additional experiments are necessary to compare the kinetics of desensitization of the tethered agonist to those of ACh. Responses measured by two-electrode voltage clamp are ill-suited to a detailed analysis of the kinetics or extent of desensitization, and characterization of tethered agonist responses by rapid perfusion of Cys mutant nAChRs in excised patches will better quantify receptor desensitization. In addition, it will be important to determine by single-channel analyses the single-channel conductance and gating properties of the Cys mutant receptors in the presence of ACh or tethered agonists. In contrast to most positions that were studied, no modification of αY93C resulted in nAChR activation, and the modifications fully inhibited subsequent ACh responses. This might occur if the modification resulted in receptor desensitization without detectable activation. However, consideration of the structure of the nAChR in the absence of agonist, which we discuss later, suggests that it is more likely that modification of αY93C in the absence of agonist results in neither activation nor desensitization.

Length Requirements for Tethered Agonists: Experiment versus Homology Modeling. Our experimental studies established that there were stringent length requirements for nAChR activation by $-SC_nTMA$'s tethered at substituted Cys residues in the γ and δ subunits. Tethered $-SC_2TMA$ tethered at γL119C/δL121C acted as an agonist, producing sustained currents that were 25% as large as the maximal response to ACh, while tethered $-SC_1TMA$ did not activate and inhibited subsequent ACh responses. Tethered $-SC_2$-

TMA did not activate from other positions in binding site segment E, and to our surprise, it did not activate from γW55C/δW57C. Tethered $-SC_4$TMA at γW55C/δW57C did activate, although as we discussed above, this longer tether acted at this position and at most others as a gating modifier rather than as a tethered ligand that prevented the subsequent binding of ACh. Comparison of the experimentally determined length requirements for tethered agonist function (Table 3) with the predicted positions of the positive charge of $-SC_n$TMA's tethered at positions in the γ subunit in an nAChR homology model based upon the AChBP structure (Figure 10) reveals that the positive charge of the tethered agonist ($-SC_2$TMA at γL119C) is centered within the core aromatic box and that short tethers with the charge displaced more than 1 Å from that of TMA function as tethered antagonists [$-SC_2$TMA at γW55C (2.7 Å) and $-SC_1$TMA at γL119C (1.8 Å)]. These results suggest that the homology model is an excellent representation of the transmitter binding site in an open channel conformation rather than a desensitized conformation. The experimental results also indicate that the use of $-SC_n$TMA's as molecular rulers is complicated by their ability to act as gating modifiers, as seen for $-SC_2$TMA tethered at γE57C/δD59C and γL109C/δL111C, positions characterized by tethered charges displaced at least 2.4 and 3.0 Å, respectively, from that of TMA.

On the basis of the homology model, for $-SC_2$TMA tethered at αCys192 or αCys193 (or at αY93C, αW149C, αY198C, or αY190C), the positive charge can be positioned within 1 Å of that of TMA, but not from any of the adjacent positions. Tethered $-SC_2$TMA at αCys192 or αY198C acted as an agonist, with an apparent optimal length to produce persistent currents as large or larger than the maximal ACh currents. The lack of gating by $-SC_n$TMA's tethered at αV188C, αT191C, or αP194C is also consistent with the homology model [as is the lack of gating from Cys-substituted α195−197 or α199−201 (*14*)]. However, there were discrepancies between the experimental results and the model. (i) For αY93C, tethered $-SC_2$TMA did not activate the nAChR, but it inhibited the ACh response, a result also seen for $-SC_1$TMA or $-SC_3$TMA and in the presence of the βL257S mutant that destabilizes the closed channel state. (ii) $-SC_2$TMA tethered at αCys193 acted as a modifier, gating the nAChR without preventing the subsequent binding of ACh. (iii) As noted above, for the αW149C and αY190C mutants, which could be studied only in the presence of the βL257S subunit, the observed responses indicated that the tethered ligands were acting as modifiers.

The inability of $-SC_2$TMA tethered at αY93C to gate the nAChR can be understood by reference to the structure of the nAChR in the absence of agonist (closed state) (*8*), i.e., the nAChR state modified when receptors are exposed to $MTSC_n$TMA's in the absence of agonist. Comparison of the *Torpedo* nAChR structure in the absence of agonist with the homology model based upon the AChBP reveals that the differences in transmitter binding site structures (Figure 10C,D) are largely limited to the α subunit and include a reorientation of the turn containing αCys192/αCys193 between β strands 9 and 10 that brings αCys192/αCys193 in the homology model ~5 Å closer to γTrp55 or γLeu119 in the antiparallel β strands that make up the β sheet in γ and δ subunits that form the entry to the ACh binding pocket. In the closed state structure, the side chain of α93, while accessible for modification, is oriented toward αAsp200 and largely shielded from the γ−δ subunit interface by the side chains of αTyr190 and αTyr198. For this structure, it is not surprising that a positive charge tethered at αY93C is unable to stabilize a binding site structure similar to that of the AChBP. In addition, since the αC192S and αC193S substitutions prevent the formation of αcystine192/193, it is likely that these substitutions produce changes in structure not predicted by either available structure. The fact that $-SC_2$TMA inhibits ACh responses when tethered at αCys192, but not at αCys193, suggests that the orientation of αCys193 deviates from the orientation predicted in the homology model.

ACKNOWLEDGMENT

We thank Luis de la Torre for preliminary experiments characterizing the effects of reducing and oxidizing agents on the responses of the αC192S mutant nAChR. We also thank Galo Garcia, III, for useful comments about the manuscript.

REFERENCES

1. Corringer, P.-J., Le Novere, N., and Changeux, J.-P. (2000) Nicotinic receptors at the amino acid level, *Annu. Rev. Pharmacol. Toxicol. 40*, 431−458.
2. Karlin, A. (2002) Emerging structure of the nicotinic acetylcholine receptors, *Nat. Rev. Neurosci. 3*, 102−114.
3. Colquhoun, D., and Sivilotti, L. G. (2004) Function and structure in glycine receptors and some of their relatives, *Trends Neurosci. 27*, 337−344.
4. Sine, S. M., and Engel, A. G. (2006) Recent advances in Cys-loop receptor structure and function, *Nature 440*, 448−455.
5. Brejc, K., van Dijk, W. J., Klaassen, R., Schuurmans, M., van der Oost, J., Smit, A. B., and Sixma, T. K. (2001) Crystal structure of AChBP reveals the ligand-binding domain of nicotinic receptors, *Nature 411*, 269−276.
6. Celie, P. H. N., van Rossum-Fikkert, S. E., van Dijk, W. J., Brejc, K., Smit, A. B., and Sixma, T. K. (2004) Nicotine and carbamylcholine binding to nicotinic acetylcholine receptors as studied in AChBP crystal structures, *Neuron 41*, 907−914.
7. Unwin, N., Miyazawa, A., Li, J., and Fujiyoshi, Y. (2002) Activation of the nicotinic acetylcholine receptor involves a switch in conformation of the α subunits, *J. Mol. Biol. 319*, 1165−1176.
8. Unwin, N. (2005) Refined structure of the nicotinic acetylcholine receptor at 4 Å resolution, *J. Mol. Biol. 346*, 967−989.
9. Zhang, Y., Chen, J., and Auerbach, A. (1995) Activation of recombinant mouse acetylcholine receptors by acetylcholine, carbamylcholine and tetramethylammonium, *J. Physiol. 486*, 189−206.
10. Akk, G., and Auerbach, A. (1996) Inorganic, monovalent cations compete with agonists for the transmitter binding site of nicotinic acetylcholine receptors, *Biophys. J. 70*, 2652−2658.
11. Damle, V. N., McLaughlin, M., and Karlin, A. (1978) Bromoacetylcholine as an affinity label of the acetylcholine receptor from *Torpedo californica*, *Biochem. Biophys. Res. Commun. 84*, 845−851.
12. Chabala, L. D., and Lester, H. A. (1986) Activation of acetylcholine receptor channels by covalently bound agonists in cultured rat myoballs, *J. Physiol. 379*, 83−108.
13. Sullivan, D. A., and Cohen, J. B. (2000) Mapping the agonist binding site of the nicotinic acetylcholine receptor: Orientation requirements for activation by covalent agonist, *J. Biol. Chem. 275*, 12651−12660.
14. Sullivan, D., Chiara, D. C., and Cohen, J. B. (2002) Mapping the agonist binding site of the nicotinic acetylcholine receptor by cysteine scanning mutagenesis: Antagonist footprint and secondary structure prediction, *Mol. Pharmacol. 61*, 463−472.
15. Mishina, M., Tobimatsu, Y., Imoto, K., Tanaka, K.-I., Fujita, Y., Fukuda, K., Kurasaki, M., Takahashi, H., Morimoto, Y., Hirose, T., Inayama, S., Takahashi, T., Kuno, M., and Numa, S. (1985)

Location of functional regions of acetylcholine receptor α-subunit by site-directed mutagenesis, *Nature 313*, 364−369.
16. Burmeister Getz, E., Xiao, M., Chakrabarty, T., Cooke, R., and Selvin, P. R. (1999) A comparison between the sulfhydryl reductants tris(2-carboxyethyl)phosphine and dithiothreitol for use in protein biochemistry, *Anal. Biochem. 273*, 73−80.
17. Karlin, A. (1969) Chemical modification of the active site of the acetylcholine receptor, *J. Gen. Physiol. 54*, 245s−264s.
18. Kao, P. N., and Karlin, A. (1986) Acetylcholine receptor binding site contains a disulfide cross-link between adjacent half-cystinyl residues, *J. Biol. Chem. 261*, 8085−8088.
19. Stauffer, D. A., and Karlin, A. (1994) Electrostatic potential of the acetylcholine binding sites in the nicotinic receptor probed by reactions of binding-site cysteines with charged methanethiosulfonates, *Biochemistry 33*, 6840−6849.
20. Labarca, C., Nowak, M. W., Zhang, H. Y., Tang, L. X., Deshpande, P., and Lester, H. A. (1995) Channel gating governed symmetrically by conserved leucine residues in the M2 domain of nicotinic receptors, *Nature 376*, 514−516.
21. Filatov, G. N., and White, M. M. (1995) The role of conserved leucines in the M2 domain of the acetylcholine receptor in channel gating, *Mol. Pharmacol. 48*, 379−384.
22. Zhong, W. G., Gallivan, J. P., Zhang, Y. N., Li, L. T., Lester, H. A., and Dougherty, D. A. (1998) From ab initio quantum mechanics to molecular neurobiology: A cation-π binding site in the nicotinic receptor, *Proc. Natl. Acad. Sci. U.S.A. 95*, 12088−12093.
23. Li, L. T., Zhong, W. G., Zacharias, N., Gibbs, C., Lester, H. A., and Dougherty, D. A. (2001) The tethered agonist approach to mapping ion channel proteins toward a structural model for the agonist binding site of the nicotinic acetylcholine receptor, *Chem. Biol. 8*, 47−58.
24. Steudel, R. (1975) Properties of sulfur−sulfur bonds, *Angew. Chem., Int. Ed. 14*, 655−664.
25. Thornton, J. M. (1981) Disulphide bridges in globular proteins, *J. Mol. Biol. 151*, 261−287.
26. Creighton, T. E. (1988) Disulphide bonds and protein stability, *BioEssays 8*, 57−63.
27. Hazes, B., and Dijkstra, B. W. (1988) Model building of disulfide bonds in proteins with known three-dimensional structure, *Protein Eng. 2*, 119−125.
28. Neubig, R. R., Boyd, N. D., and Cohen, J. B. (1982) Conformations of *Torpedo* acetylcholine receptor associated with ion transport and desensitization, *Biochemistry 21*, 3460−3467.
29. Jackson, M. B. (1986) Kinetics of unligated acetylcholine receptor channel gating, *Biophys. J. 49*, 663−672.
30. Chakrapani, S., Bailey, T. D., and Auerbach, A. (2003) The role of loop 5 in acetylcholine receptor channel gating, *J. Gen. Physiol. 122*, 521−539.
31. Akk, G., and Steinbach, J. H. (2003) Activation and block of mouse muscle-type nicotinic receptors by tetraethylammonium, *J. Physiol. 551*, 155−168.

BI060686T